CHAPTER 16

KINEMATICS IN THE CRESTS OF STORM WAVES

George Z. Forristall*

ABSTRACT

Uncertainty about kinematics in the crests of high waves has prevented random wave simulation from being accepted as a reliable method for computing wave forces for platform design. A theoretically defensible method of calculation for wave crest kinematics has been developed recently. The method produces a potential function which fits the kinematic boundary condition specified by second order wave theory and is thus named the Kinematic Boundary Condition Fitting (KBCF) method. KBCF agreed well with measurements of mechanically generated irregular waves made by a laser Doppler current meter in a wave tank. In order to obtain further data during high, short crested storm waves, instruments for the Fulmar Wave Crest Kinematics (FULWACK) experiment were installed in the North Sea early in November 1981. During a storm later in that month, good velocity measurements at heights up to 25 feet above mean water level were obtained in over 30 waves. For comparison with this data, KBCF was extended to three dimensions. Statistics of the velocities thus simulated agreed well with statistics of the measurements. KBCF has thus been verified as a accurate method for simulating the kinematics of natural storm waves.

INTRODUCTION

Monte Carlo simulations are needed to model the dispersive and directionally spread nature of ocean waves. Forristall (1981) showed that such simulations agreed well with velocity measurements made below mean water level in storms at sea. However, heuristically motivated modifications to linear theory are necessary to produce realistic velocities above mean water level, and it is not clear which modification is best.

Forristall (1985) then developed a new method for computing the kinematics of irregular waves based on the numerical calculation of a potential function with a given kinematic free surface boundary condition (KBCF). The boundary condition was specified correct to second order using the intermediate depth interaction equations developed by Sharma and Dean (1979). Measurements made by Bosma and Vugts (1981) using a laser Doppler current meter in the Delft Hydraulics Laboratory wave tank were particularly appropriate for testing KBCF theory. Velocities were measured one standard deviation of wave height above mean water level as well as below mean water level. The waves were mechanically generated and unidirectional. The wave staff record could thus be used to specify the phases of the component wavelets, and only a two-dimensional potential function had to be calculated. The agreement found by Forristall (1985) between measured and simulated velocities was excellent. There was also good agreement between the statistics of measured and simulated velocities when only the spectral density of the waves was specified as input to the simulations.

Since KBCF is derived from the equations of wave motion using defensible assumptions, the extrapolation from laboratory scale to storm waves can be made with some confidence. Still, there is no substitute for verification with measurements made in natural short crested waves with heights comparable to those used in design. In response to this need, the Fulmar Wave Crest Kinematics (FULWACK) experiment was conducted in the central North Sea during the winter of 1981-82. Five electromagnetic current meters were mounted on taut wires stretched outboard of the north face of the Fulmar platform. Two of the meters were below mean water level and gave an estimate of the directional spectrum when used in conjunction with a wave staff. The other three meters were at nominal heights of 6, 16, and 26 feet above mean water level and gave velocity records when they were briefly immersed in the crests of high waves.

Shortly after the instruments became operational in November 1981, a pair of storms produced the most severe conditions observed during the winter. Data from these storms were digitized, and the velocity records from the second storm were used to verify KBCF wave theory. We first calculated directional wave spectra from the records. The velocity data from the wave crests were then compared with Chappelear (1961) regular wave theory and with the empirical modifications of linear theory known as stretching and extrapolation.

KBCF theory was originally developed for two-dimensional waves, and the three-dimensional problems required substantially more computational effort. The code that was developed uses the vector processing

* Shell Development Co., Box 481, Houston, TX 77001

and large storage capabilities of the Cray computer. Statistics of peak velocities simulated by the three-dimensional KBCF compare very well to the statistics of the measured velocities.

KBCF wave theory agrees with both high quality laboratory measurements and measurements made in extreme waves in a natural seaway. In the last section, we consider how the realistic simulations it produces can be used for structural design.

THE FULWACK EXPERIMENT

The Fulmar platform is located in block 31/16 in the central North Sea, within sight of the Auk platform in the same block. The platform is in 270 feet of water approximately 170 miles east of Dundee, Scotland. A Baylor wave staff and five Marsh-McBirney model 524 electromagnetic current meters were mounted just outside the north face of the platform as shown in Figure 1. The current meter support system consists of a wire rope stretched around upper and lower sheaves to form a taut wire loop. Frames for the current meters and their cables were clamped to one side of the loop and lowered to position by rotating the top sheave. The response of the taut wire system was investigated using the finite difference program described by Forristall and Hamilton (1978). Since the taut wires were clamped to the spider deck at the 20 foot level, current meters 3 and 4 were predicted to have the biggest motion: about 3 feet in a 75 foot wave. The natural periods of the taut wire sections above and below the clamps were each close to 0.5 sec.

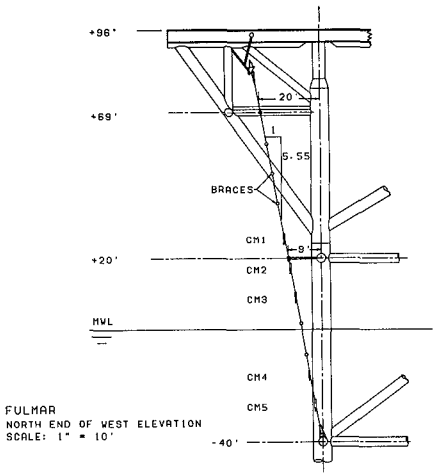

Figure 1.

The nominal locations of current meters 1–5 respectively were 26, 16, and 6 feet above mean water level, and 18 and 28 feet below it. During the data analysis, the water level on the wave staff was used to give the water level relative to the current meters. Float switches were also installed next to the top three current meters to determine the precise times of their immersions. Laboratory test showed that the response time of the switches was approximately 0.2 sec. However, the strong flow during storm waves apparently held the floats down part of the time, and the immersion times were usually determined from the wave staff signal.

The current meter axes were aligned with the platform so that a positive x-axis response indicated flow towards platform east and a positive y-axis response indicated flow toward platform north. Platform north is 18.5° counterclockwise from true north, so positive x-axis response indicated flow toward 71.5° true.

A J-Tec vortex shedding anemometer was mounted above the crown block on the drilling derrick, 345 feet above mean water level. Some possible blockage might be caused by the flare stack located to the south-southeast of the derrick. We intended to mount the anemometer so that the direction reading

would be in degrees from true north, but later comparisons between visual observation of vane position and instrument output indicated that about 15° should be subtracted from the measured directions.

The signal conditioning and recording system was manufactured by Evans-Hamilton Inc. and was housed in an instrument shelter located at the northeast corner of the cellar deck. All signals except those from the immersion switches were passed through 4 pole Butterworth filters with a cutoff frequency of 3.0 Hz. These filters replaced the output filters normally supplied with the Marsh-McBirney current meters. The Butterworth filters give a sharper cutoff as well as producing equal phase lags in the wave staff and current meter signals.

The conditioned signals were recorded on 14 channel Geotech FM analog tape recorders. Two recorders were used to give redundancy in the event of mechanical failure of one of the recorders. The recorders ran continuously at 0.03 inch/sec, and had flat frequency response to above 4 Hz. The system switched from data recording to an automatic calibration mode once each hour. During the two phases of the calibration, which lasted two minutes each, calibration signals were substituted for data and recorded through the same signal conditioning circuits. The wave staff calibration was given by two shorter bars operated by relays. The electromagnetic current meters included an internal calibration feature which fed a portion of the magnet driver excitation voltage through the channel amplifiers.

Data from two storms in November 1981 were digitized for detailed analysis. During the analog to digital conversion, the field recorded tapes were played at 3.75 inch/sec, giving a playback/field speed ratio of 125. The digitization rate was 500 Hz at playback speed, equivalent to 4 Hz at field speed. The A/D circuit had a resolution of 12 bits or one part in 4096. To avoid aliasing, the wind, wave, radar, and current meter 4 and 5 signals were filtered using 4 pole Butterworth filters with a cutoff frequency of 200 Hz at playback speed or 1.6 Hz at field speed. The immersion switch channel and current meters 1–3 were not filtered because of the intermittent nature of the signals.

The digital data were calibrated using the hourly calibration values. For each hour of field data, 6 records containing 2048 time-steps of 14 channels each were written. The effects of both the signal conditioning filters used in the field and the anti-aliasing filters were removed by multiplying the Fourier transforms of the signals by the transfer function

$$T(f) = (\tilde{f} - p_1)(\tilde{f} - \bar{p}_1)(\tilde{f} - p_2)(\tilde{f} - \bar{p}_2) \tag{1}$$

where

$$p_1 = -.3827 + .923872i,$$

$$p_2 = -.923873 + .3827i,$$

and

$$\tilde{f} = f/f_c,$$

f_c is the cutoff frequency for either of the four pole Butterworth filters, and overbars denote complex conjugation. For the filters used in the instrumentation system $f_c = 3.0$ Hz, and for the filters used during digitization $f_c = 1.6$ Hz.

Components above the cutoff frequency were removed. The current meter records were also corrected for the slight nonlinearity and non-cosine response established by tank testing of meters of this type. The calibrated current meter signal was divided by the factor r, given by

$$\begin{aligned} r &= \beta(1 - \alpha\sin 2\theta), \\ \beta &= 0.87 \quad \text{for} \quad Re < 2.51 \times 10^4 \\ &= 1.0612 - 4795/Re \quad \text{for} \quad 2.51 \times 10^4 < Re < 7.84 \times 10^4 \\ &= 1.0 \quad \text{for} \quad Re > 7.84 \times 10^4 \\ \alpha &= 0.083 - 1.5 \times 10^{-6} Re \quad \text{for} \quad Re < 5.52 \times 10^4 \\ &= 0 \quad \text{for} \quad Re > 5.52 \times 10^4. \end{aligned} \tag{2}$$

Re is the Reynolds number of the flow around the spherical sensor (4" in diameter), and θ is the direction of the flow with respect to an electrode.

THE NOVEMBER 1981 STORMS

The FULWACK system operated from November 12, 1981 to April 29, 1982, but two storms in the middle of November 1981 produced the most severe wave conditions during the experiment. The first storm developed from a low which formed east of Newfoundland and expanded as it moved to the North Sea with a minimum pressure of 972 mb. Thirty-six hours later, another low formed and followed the same track. It suddenly deepened, reaching 975 mb near the Faroe Islands (Mariner's Weather Log, 1982). The slow forward motion of the storm was partly responsible for the very high waves observed in the North Sea on November 24.

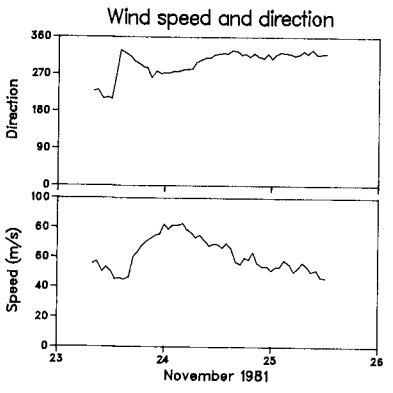

Figure 2.

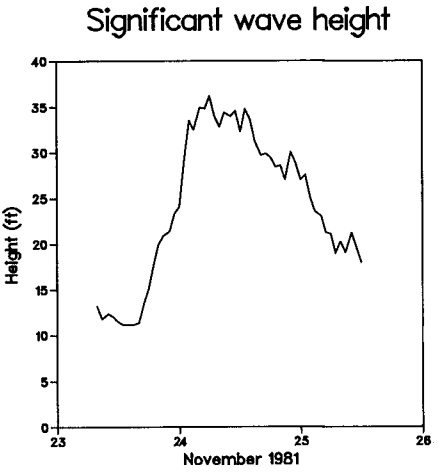

Figure 3.

Figure 2 shows the wind speed and direction measured by FULWACK during the second storm, and Figure 3 shows the significant wave height. The winds are as measured from the location at the top of the derrick. The wind speed and direction were averaged over 6 data records, giving approximately one hour averages. The wind direction has been corrected for the 15° error in instrument alignment discussed above. The wind speed reached a brief peak of 77 miles/hr on the afternoon of November 20. Then on November 24, the wind speed was near its peak of 82 miles/hr for several hours, and the direction was nearly constant.

The significant wave height in Figure 3 was calculated as four times the standard deviation of the wave signal. On November 20, the peak significant wave height was 30 feet, and on November 24 it was 36 feet. Figure 4 is a photograph taken by Mr. Mike Philpot from the Borgland Dolphin accommodations semisubmersible on November 24, illustrating the severity of the conditions. The view is toward the north face of the platform which the wave crest is approaching. The wave crest appears to be considerably higher than the spider deck located at 20 feet above mean sea level.

With two exceptions, the sensors and recording system worked very well during the storms. The y-axis of current meter 3 did not operate in either storm, and a radar wave gage installed as part of another experiment but recorded on the FULWACK system failed during the first storm.

Figure 4. A large wave on November 24

WAVE SPECTRA

We calculated directional spectra for each hour of digitized data using the methods of Forristall *et al* (1978). The information on wave direction available from a wave staff and current meter is equivalent to that from a pitch and roll buoy. It does not provide very sharp directional resolution in the sense of separating two directional peaks at one frequency. However, it can provide very good information on the mean direction of travel and amount of directional spreading for waves in each frequency band.

The co-spectra between the wave staff and current meters 4 and 5 were used to find the best estimates of the parameters in the function

$$S(f,\theta) = S(f)N(s)\cos^{2s}(\theta - \theta_o/2) \tag{3}$$

The mean direction of travel, θ_o and the spreading parameter, s, are both functions of frequency. The function $N(s)$ is included to normalize the integral of the spreading function to unity. The spectral density as a function of frequency alone, $S(f)$, was calculated directly from the wave staff data. We also calculated the rms spread, skewness, and kurtosis of the direction distribution.

With a time step of .25 sec and a record length of 2048 points, the raw spectra from a fast Fourier transform have a frequency resolution of 1/512 Hz. We took averages over 5 frequencies and ensembles of 6 spectra to give spectra with 60 degrees of freedom and a resolution of 0.01 Hz.

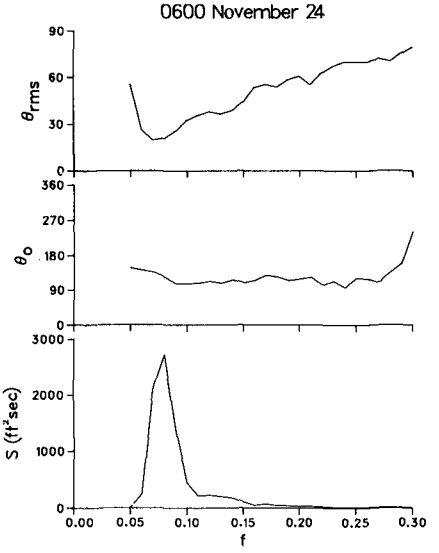

Figure 5. Directional wave spectrum at 0600

Although the energy level of the spectra varied during the storm, their directional characteristics were quite constant. Figure 5 shows the directional spectrum for 0600 on November 24, the time at which the significant wave height reached its maximum of 36.20 feet. The bottom panel of the figure shows the power spectrum, the middle panel shows the mean direction of travel, and the top panel shows the rms directional spread, all as a function of frequency. The power spectrum is unimodal with a peak at 0.08 Hz. The mean direction of travel is nearly constant with frequency, with the waves traveling toward 110° true in the mean. The rms spread is smallest at the peak of the spectrum and increases with frequency. The rms spread is related to the parameter s in equation (3) by

$$s = 2/\theta_{rms}^2 - 1 \tag{4}$$

where θ_{rms} is expressed in radians. The rms spread is a more physically appealing measure of the spreading while equation (3) is useful when a definite form of the spreading function is needed. The qualitative features of the spectrum shown in Figure 5 are typical of those computed throughout the storm.

The calculation of directional spectra from wave staff and current meter data is based on linear wave theory and gives a check on the accuracy of linear theory. The average ratios of measured to linearly predicted velocities were 0.97 for current meter 4 and 0.99 for current meter 5.

CREST VELOCITY MEASUREMENTS

The main purpose of the FULWACK experiment was to obtain velocity measurements at locations high above mean sea level where the current meters would be immersed only briefly. The behavior of the electromagnetic current meters during intermittent immersion is therefore important. Before installing the instruments on Fulmar, we conducted some immersion tests in a recirculating flume. Figure 6 shows the data recorded during one of the tests where the flow was parallel to the y-axis of the meter. Both channels of the meter had a large noise spike immediately after immersion, but then settled to the correct response after 0.6 second. The characteristics of the noise seem related to the output filter used on the current meter, which was the same in the tests and FULWACK.

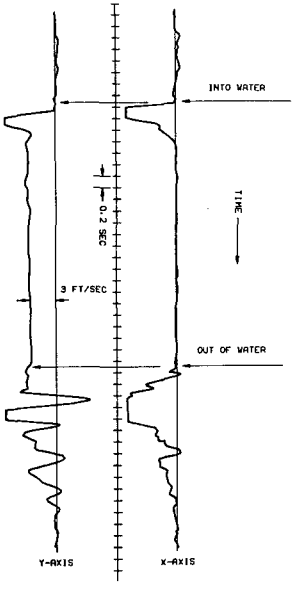

Figure 6. Current meter immersion test

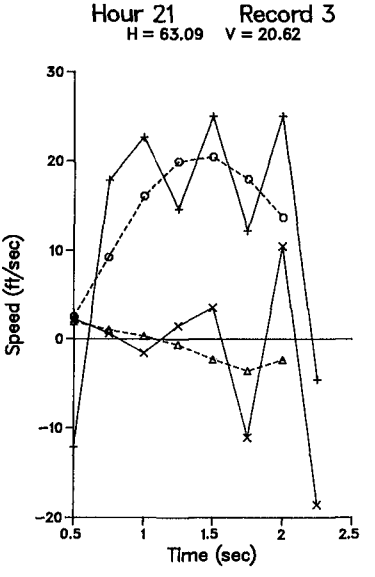

Figure 7. Kinematics of the largest wave

The flume tests indicated that reliable results could be expected only after the meter was immersed at least 0.5 sec. In order to have a few good data points for averaging or curve fitting, we selected only those waves for which a meter was immersed during at least 7 digitized samples. The meter was thus immersed longer than 1.5 sec. Applied to the top current meter, this selection scheme produced 31 waves for study from the November 24 data.

Figure 7 illustrates the quality of the actual data during the highest wave recorded. The solid line marked with + symbols is the output from the x-axis of the top current meter, and the solid line marked with × symbols is the output from the y-axis. All data points during the immersion are shown, and the origin of the time axis is arbitrary. The data has rapid oscillations and spikes with frequencies on the order of 2 Hz. This behavior was not observed in the flume tests and is not expected to be due to wave kinematics, since there is little wave energy at these frequencies. Since the natural frequency of the taut wire system is ncar 2 Hz, it is likely that the oscillations are due to relative motion between the meter and the water. Small amplitude motions can cause large relative velocities at high frequencies. The oscillations were removed by filtering.

After some experimentation with curve fitting and various smoothing schemes, we decided that the

best method for removing the noise would be a simple filter. The velocity components were filtered at $f_c = 0.5$ Hz using a filter with the amplitude response of the four pole Butterworth filter in equation (1), but with zero phase lag. The filter was applied in the frequency domain, so it was simply a real transfer function with amplitude equal to the modulus of the Butterworth transfer function. The result of the filtering is illustrated by the dashed lines in Figure 7. The filtered components seem to give a credible version of the wave velocity while eliminating the physically unrealistic oscillations.

REGULAR WAVE THEORY

The velocity components were combined vectorially and the maximum speed in the crest of each wave found for comparison with wave theories. For the wave in Figure 7, this maximum velocity was 20.62 ft/sec. The maximum speed recorded during the storm at the top meter was 21.47 ft/sec.

We first compared the measurements with the predictions of regular wave theory using the high order numerical solution of Chappelear (1961). This theory gives an excellent fit to the regular wave boundary conditions. For waves of the moderate steepness and water depth encountered by FULWACK, the solution does not differ significantly from that given by Stokes fifth order theory.

For each of the 31 waves, the period and height were computed using the zero downcrossing definition applied to the wave staff record. Figure 8 gives a comparison between the measured maximum speeds at current meter 1 and the speeds calculated by Chappelear theory. The scatter between the measured and theoretical peak speeds is considerable. The theoretical speeds are also biased about 15% to overprediction. These results are consistent with those from previous measurements made below mean water level.

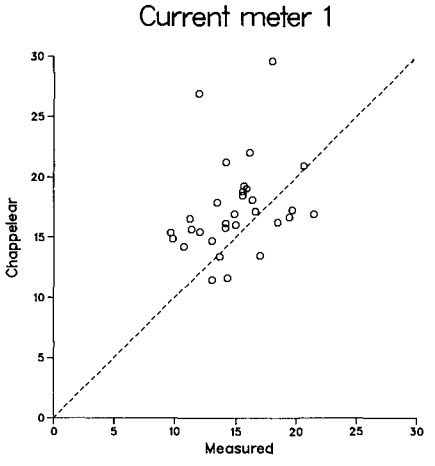

Figure 8. Peak speeds in single waves

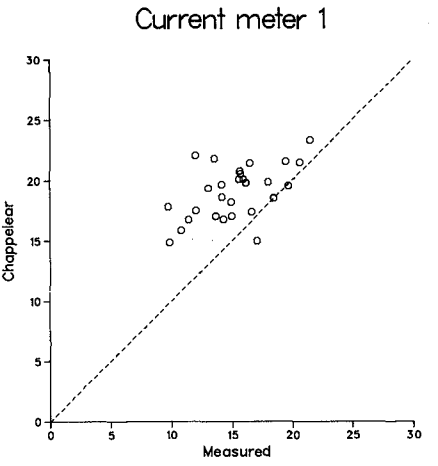

Figure 9. Peak speeds with crest defining wave

Two of the Chappelear velocities in Figure 8 are conspicuously higher than the others. These outlyers are apparently due to short zero crossing periods which do not represent the important frequencies in the wave spectrum. Daemrich and Kohlhase (1980) have suggested another way of selecting the parameters for regular waves which reduced the scatter between theory and their measurements of unidirectional irregular waves in a tank. They defined the wave by the height of the crest and the period of the crest between zero crossings. Since they used linear wave theory, the wave height and period were twice the height and period of the crest. The FULWACK waves were steep enough so that the use of nonlinear theory was advisable, so we modified Chappelear theory to converge to a specified crest height and period rather than the crest to trough height. The wave parameters were selected from the same set of 31 waves as before, and the wave by wave comparison of maximum velocities is shown in Figure 9. The scatter has indeed been reduced somewhat, mostly by the elimination of the two outlyers. The bias remains and is, in fact, larger. The improvement in the comparison is not nearly so much as reported by Daemrich and Kohlhase (1980), presumably because of the complicating effect of directional spreading in the present data.

MODIFIED LINEAR THEORIES

Forristall *et al* (1978) showed that linear simulation of the directional wave spectrum could produce velocity probability distributions which agreed well with measurements below mean water level. However, the linear superposition principle breaks down above mean water level. Empirical modifications such as stretching and extrapolation have thus been necessary to produce reasonable results. Comparisons of these methods with measurements (Forristall, 1981) have not been completely conclusive.

Wave kinematics are stretched by moving the level at which $z = 0$ in the linear wave expansion to the instantaneous free surface. In practice, a coordinate transformation is performed after the linear waves are superposed. Kinematics are extrapolated by taking the linear simulation up to mean water level and then continuing upward using the rate of increase with z calculated just at mean water level.

The simulations were made using a fast Fourier transform technique with random phases selected for each Fourier line. There were 30 directional bands at each frequency. The simulations were based on the directional spectra measured from 0200-2300 GMT. Records having the same length as the measurements were produced, and they were analyzed using the same routine. This single, literal unconditioned simulation of the storm should have the same statistical variability as the measurements. Thus, wave by wave comparisons could not be performed, and, in fact, a slightly different number of simulated waves met the immersion criteria.

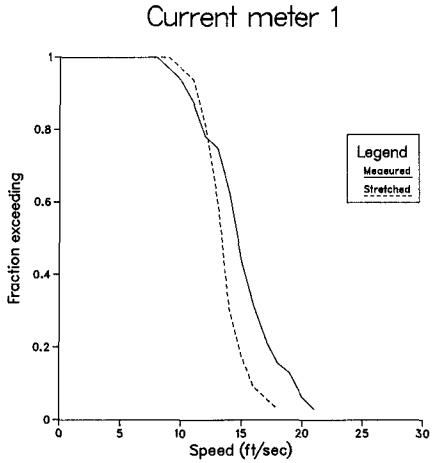

Figure 10. Distributions of measured and stretched speeds

Figure 10 shows the peak speed distribution from the stretched and simulation compared with the measurements at current meter 1. The stretched simulation agrees well with the measurements at lower velocities but is somewhat below the measurements at lower probabilities. The speeds from the extrapolated simulations (not shown) were clearly too high. These results are consistent with those found from a study of MaTS measurements in the Delft Hydraulics Laboratory. However, they disagree with the results of the measurements made at the Exxon Ocean Test Structure (OTS) as discussed by Forristall (1981).

KBCF

The Kinematic Boundary Condition Fitting (KBCF) method was developed to put the calculation of random wave kinematics on a rigorous basis. The kinematic field should be given by a potential function which satisfies Laplace's equation in the interior and the kinematic and dynamic boundary conditions on the free surface. The basic idea of KBCF is that if the shape and time derivative of the surface are known, the kinematic free surface boundary condition alone is enough to completely specify the potential as the solution to a Neumann problem. The solution can be calculated easily enough by numerical iteration. Forristall (1985) found that a specification of the surface correct to second order was sufficient to produce a solution which agreed excellently with the MaTS measurements in the Delft wave tank.

For comparison with the FULWACK measurements and for design use, it is necessary to extend KBCF to three dimensions. The second order wave interactions for infinite water depth were calculated by Longuet-Higgins (1963), and the calculations were extended to intermediate water depth by Sharma and Dean (1979). We reproduce the latter result for completeness. Let the first order water surface be given by

$$\eta = \sum_{n=1}^{N} a_n \cos(\kappa_n x - \sigma_n t + \epsilon_n) \tag{5}$$

where t is time, x is the position vector in the plane, σ_n. ϵ_n and κ_n are, respectively, the radian frequency, phase, and vector wavenumber of wavelet n, and a_n is its amplitude. The frequencies and wavenumbers are related by the linear dispersion equation

$$\sigma_n^2 = g|\kappa_n|\tanh|\kappa_n|d \tag{6}$$

where g is the acceleration of gravity and d is the water depth.

The second order correction to the wave surface given by Sharma and Dean (1979) is then

$$\eta^{(2)} = 1/4 \sum_{i=1}^{N}\sum_{j=1}^{N} a_i a_j \{K^- \cos(\psi_i - \psi_j) + K^+ \cos(\psi_i + \psi_j)\} \tag{7}$$

where

$$K^- = [D_{ij}^- - (\kappa_i \kappa_j + R_i R_j)]\sqrt{R_i R_j} + (R_i + R_j)$$

$$K^+ = [D_{ij}^+ - (\kappa_i \kappa_j - R_i R_j)]\sqrt{R_i R_j} + (R_i + R_j)$$

$$D_{ij}^- = \frac{(\sqrt{R_i} - \sqrt{R_j})\{\sqrt{R_j}(\kappa_i^2 - R_i^2) - \sqrt{R_i}(\kappa_j^2 - R_j^2)\}}{(\sqrt{R_i} - \sqrt{R_j})^2 - \kappa_{ij}^- \tanh\kappa_{ij}^- d} +$$
$$+ \frac{2(\sqrt{R_i} - \sqrt{R_j})^2(\kappa_i \kappa_j + R_i R_j)}{(\sqrt{R_i} - \sqrt{R_j})^2 - \kappa_{ij}^- \tanh\kappa_{ij}^- d}$$

$$D_{ij}^+ = \frac{2(\sqrt{R_i} + \sqrt{R_j})^2(\kappa_i \kappa_j - R_i R_j)}{(\sqrt{R_i} + \sqrt{R_j})^2 - \kappa_{ij}^+ \tanh\kappa_{ij}^+ d} +$$
$$+ \frac{(\sqrt{R_i} + \sqrt{R_j})\{\sqrt{R_i}(\kappa_j^2 - R_j^2) + \sqrt{R_j}(\kappa_i^2 - R_i^2)\}}{(\sqrt{R_i} + \sqrt{R_j})^2 - \kappa_{ij}^+ \tanh\kappa_{ij}^+ d}$$

$$\kappa_{ij}^- = |\kappa_i - \kappa_j|$$

$$\kappa_{ij}^+ = |\kappa_i + \kappa_j|$$

$$R_i = |\kappa_i|\tanh|\kappa_i d| = \sigma_i^2/g$$

$$\psi_i = \kappa_i x - \sigma_i t + \epsilon_i.$$

For infinite water depth, equation (7) reduces to equation (3.7) of Longuet-Higgins (1963) except that the latter equation is missing a factor of $1/2$. The skewness kernel is defined as $(K^- + K^+)/4$ and is a measure of the strength of the second order interaction. It is a function of the frequencies of the two interaction wavelets as well as their angular separation and the water depth. The strength of the interaction is much greater in shallow water, matching the observation that the wave profile is more skewed in shallow water. It is interesting to note that for shallow water the peak of the interaction is not for colinear wavelets, but for wavelets separated by a small angle.

The computations implied by equation (7) can be performed for a spectrum specified either in the frequency or wavenumber domain. The input spectrum is usually specified in the frequency domain, but the numerical iteration which produces the potential function is performed over a spatial grid. It is thus most convenient to transform the directional spectrum to the wavenumber domain at the start of the calculations and then transform to the spatial grid.

The input spectra from FULWACK were given for frequencies in the range $0.050 \leq f \leq 0.340$. The wavenumber grid has a resolution $\Delta\kappa = 0.002ft^{-1}$. The wavenumbers are given by $(K_x\Delta\kappa, K_y\Delta\kappa)$ where $-63 \leq (K_x, K_y) \leq 63$ so that wavenumbers up to $0.1260ft^{-1}$ can be represented. This high wavenumber cutoff corresponds closely to the high frequency cutoff in the input spectrum. Negative wavenumber components must be included since wavelets in the input spectrum can propagate in any direction.

The program begins with a linear random simulation of the type described by Forristall (1981). Linear wavelets are specified at a frequency resolution $\Delta f = 1/512$ Hz and an angular resolution $\Delta\theta = 12^o$. The amplitude of each wavelet is taken from the given directional spectrum, and the phases are taken from a uniform random distribution. The amplitude and phase are then transferred to the proper location in the wavenumber grid.

The interactions of the wavelets are then calculated according to equation (7). If the two interaction wavelets are in close to the same direction and have large wavenumbers, the interaction term at the sum of their wavenumbers will lie outside the wavenumber grid. Wavelets traveling against the main direction of propagation are expected to be small. We thus calculated the interactions only for wavenumbers $-31 \leq (K_x, K_y) \leq 31$. Even then, the calculations are formidable. There are 63 points which satisfy that inequality so approximately 16×10^6 interactions must be calculated. Because of this and the large three-dimensional grid which is used to calculate the potential function, the computations were done on a Cray computer.

The amplitudes and phases of the first and second order wavelets in wavenumber space are transformed to the spatial grid using a fast Fourier transform which was coded to take advantage of the vector processing capabilities of the Cray and is very efficient. Two transforms are taken, first by rows and then by columns. To produce better spatial resolution, we took transforms of length 256 instead of 128. The high wave number terms were set equal to zero. The spatial resolution is then

$$\Delta x = 2\pi/256\Delta\kappa = 12.27\text{ft.} \tag{8}$$

Only the 64×64 grid surrounding $(x, y) = (0, 0)$ is calculated since this gives a large enough area for the solution of the potential function.

The KBCF solution also requires specification of η_x and η_t on the grid. These quantities are easily calculated by differentiation of equations (5) and (7), and transformed in the same way as η. An initial guess for the potential function is given by the potential due to the linear waves, again computed by successive Fourier transforms in space.

A potential function which is consistent with the surface defined correct to second order can now be calculated. Define the potential ϕ such that the velocity components (u, v, w) in the (x, y, z) directions are given by

$$\begin{aligned} u &= -\phi_x \\ v &= -\phi_y \\ w &= -\phi_z \end{aligned} \tag{9}$$

The potential function satisfies Laplace's equation

$$\phi_{xx} + \phi_{yy} + \phi_{zz} = 0 \tag{10}$$

in the interior of the fluid. At the free surface η the kinematic boundary condition is

$$\eta_t + \phi_z - \phi_x\eta_x - \phi_y\eta_y = 0 \tag{11}$$

With η, η_x, η_y, and η_t specified, equations (10) and (11) define a well posed problem which can be solved numerically. However, the wave potential should also satisfy the dynamic boundary condition

$$\eta - \phi_t/g + (\phi_x^2 + \phi_y^2 + \phi_z^2)/2g = const. \tag{12}$$

on the surface. Since the surface is only correct to second order, the numerical solution will not satisfy equation (12) perfectly. KBCF theory based on the second order surface is thus an approximation to the true solution of equations (10)-(12), and its accuracy and usefulness can be verified best through comparisons with measurements.

The potential function can be found through a successive over-relaxation solution. We define a computational grid with spacing Δx in the horizontal directions and Δz in the vertical. The grid indexes are (I, J, K) in the $(x, y, -z)$ directions. Centered difference approximations to the second derivatives are then

$$\Phi_{xx} = \{\Phi(I+1, J, K) + \Phi(I-1, J, K) - 2\Phi(I, J, K)\}/\Delta x^2 \tag{13}$$

$$\Phi_{yy} = \{\Phi(I, J+1, K) + \Phi(I, J-1, K) - 2\Phi(I, J, K)\}/\Delta x^2 \tag{14}$$

$$\Phi_{zz} = \{\Phi(I, J, K-1) + \Phi(I, J, K+1) - 2\Phi(I, J, K)\}/\Delta z^2 \tag{15}$$

At each grid point, there will be a residual given by

$$r = \Phi_{xx} + \Phi_{yy} + \Phi_{zz} \tag{16}$$

At the next step, the approximate potential is replaced by

$$\Phi'(I, J, K) = \Phi(I, J, K) + \omega r/a_{kk} \tag{17}$$

where

$$a_{kk} = 2(2/\Delta x^2 + 1/\Delta z^2) \tag{18}$$

and ω is a constant chosen to speed up convergence. On our $64 \times 64 \times 64$ grid, we used $\omega = 1.87$ and found satisfactory convergence after 100 steps.

The estimates of Φ at the new step are found successively, moving through the grid in a cyclic pattern. To make use of the vector processing capabilities of the Cray, we used what is called a "black-red" ordering. The grid is divided into "black" and "red" points in a three-dimensional checkerboard pattern. The updated potential at all the "black" points is then calculated before that at any of the "red" points. Thus the updated potential is never needed, and the calculations can proceed in parallel.

The difference scheme must be modified at the boundaries. Boundary condition (11) can be rewritten as

$$\phi_n = -\eta_t(1 + \eta_x^2 + \eta_y^2)^{-1/2} \tag{19}$$

where ϕ_n is the derivative of the potential in the direction normal to the surface. To form a finite difference estimate of the normal derivative, define

$$\begin{aligned} \epsilon_x &= \eta_x \Delta z/\Delta x \\ and \qquad \epsilon_y &= \eta_y \Delta z/\Delta x \end{aligned} \tag{24}$$

Then if ϵ_x and ϵ_y are both positive

$$\Phi_n = \{\Phi(I, J, K) - \Phi_c\}/\Delta z(1 + \eta_x^2 + \eta_y^2)^{1/2} \tag{21}$$

where

$$\Phi_c = (1 - \epsilon_y)\Phi_1 + \epsilon_y\Phi_2$$

$$\Phi_1 = (1-\epsilon_x)\Phi(I,J,K+1) + \epsilon_x\Phi(I+1,J,K+1)$$

$$\textit{and} \qquad \Phi_2 = (1-\epsilon_x)\Phi(I,J+1,K+1) + \epsilon_x\Phi(I+1,J+1,K+1)$$

The residual at the surface node (I,J,K) is then

$$r = \eta_t + \{\Phi(I,J,K) - \Phi_e\}/\Delta z \tag{22}$$

and the new potential is

$$\Phi'(I,J,K) = \Phi(I,J,K) - \omega r \Delta z \tag{23}$$

Equation (21) must be modified in an obvious way for ϵ_x or ϵ_y negative.

The bottom boundary condition is that the normal derivative of the potential is zero. The change in the solution was insignificant when the potential at the bottom was fixed equal to the linear potential. This approximation speeded convergence somewhat, and it would be reasonable to use it at a false bottom for a KBCF solution in very deep water. The potential at the lateral boundaries of the grid was also kept constant at the linear value. Forristall (1985) showed that this condition had little effect on the solution under the wave crest in the center of the grid.

COMPARISONS WITH FULWACK MEASUREMENTS

The starting point for the KBCF calculations was the linear Monte Carlo simulation that formed the basis of the stretched and extrapolated simulations. This is the same procedure that we would be following in using KBCF for design, but it means that the simulated time series is a random realization of the process defined by the directional spectrum, and wave by wave comparisons with the data are not possible. The verification of the method is thus through a comparison of speed probability distributions.

The second order interactions tend to sharpen the crests of the waves and flatten the troughs, producing a skewed sea surface. One check of the theory can thus be made by comparing the skewness of the measured and simulated profiles, where skewness is defined as

$$\alpha_3 = m_3/m_2^{3/2} \tag{24}$$

and m_2 and m_3 are the second and third moments of the wave profile. The comparison is shown in Figure 11. Skewness is not a very stable statistic: the observed value varies significantly from one record to the next. However, there is very little bias between the measured and simulated values. The agreement is in fact somewhat better than Forristall (1985) found for the MaTS wave tank data, perhaps because the finite length of the tank affected the low frequency set down under wave groups given by the subtraction term in equation (5).

The most important result of the calculations is the comparison between the measured and KBCF simulated maximum speeds at current meters 1 and 2. Figure 12 shows the comparison for current meter 1. The simulation is an essentially unbiased predictor of the measurements: the agreement is almost perfect at the 50% level. The median value of the measured maximum speed for the sample of large waves was 14.67 ft/sec at current meter 1 and 13.80 ft/sec at current meter 2. The corresponding KBCF simulations were 15.05 ft/sec at current meter 1 and 13.24 ft/sec at current meter 2, both within 5% of the measurements. The interquartile ranges (.25% to .75% exceedance) at current meter 1 were 3.67 and 3.14 ft/sec for the measurements and 2.10 and 2.17 ft/sec for the simulations. This extra variability in the measurements might be attributed to noise which remained after the filtering process. It should be recalled that the data shown in Figure 12 came only from the 31 highest waves in 12 hours of measurement in a severe storm. All of the distribution shown in the figure thus comes from the tail of the overall speed distribution. The good match of simulated and measured peak velocity statistics constitutes a verification of KBCF theory for high, directionally spread waves.

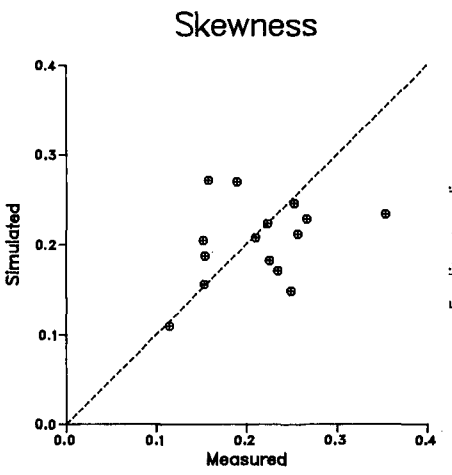

Figure 11. Wave skewness

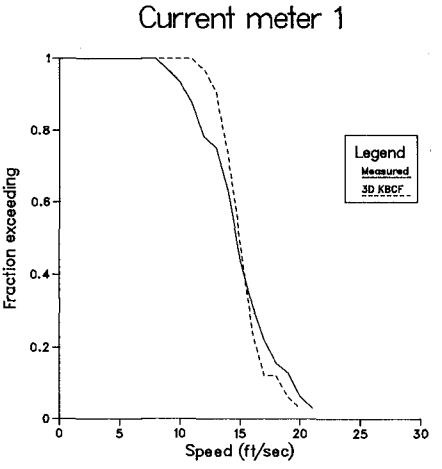

Figure 12. Distribution of measured and KBCF speeds

CONCLUSIONS

KBCF was developed as a rational approximation to the equations of motion for kinematics in the crests of irregular waves. It was compared to high quality measurements of two-dimensional waves made in a MaTS project and gave excellent results. The FULWACK experiment was designed as a full scale verification of the theory, which had to be extended to three dimensions to include the directional spreading of natural waves. Storms during November 1981 produced a good data set which included a number of waves that inundated current meters up to 26 feet above mean water level. The agreement between the velocity statistics simulated by KBCF and those measured was very good. We conclude that KBCF has been verified and is the best method of simulating the kinematic field of a complex natural seaway.

Although KBCF requires the use of a large computer, its cost is not prohibitive for simulations of individual high waves in a sea state. A number of representative waves for a design sea state could be simulated and used for static design of fixed structures. Dynamic design calculations present more of a problem, since many time steps of simulation are likely to be necessary and the cost of the simulations may become important. For these calculations and for routine design calculations on smaller computers, the best use of KBCF may be to calibrate simpler empirical models of kinematics. Rodenbusch and Forristall (1986) have developed a modification to the standard stretching algorithm which matches KBCF well in the crests of large waves.

ACKNOWLEDGEMENTS

The FULWACK project would not have been possible without the help and participation of many parts of the Shell Group. SIPM EP/23 coordinated the various activities involved. Shell Expro was extremely helpful in the design and installation of the instrument mounting system. The work of I. Middlehurst on the design and G. Grice on the installation was particularly appreciated. KSLA (Amsterdam) graciously gave us room in their instrument house, and several times loaned us spare parts from their supplies. R.C. Hamilton and T. Swarthout of Evans–Hamilton performed the instrument installation most efficiently. G. Rodenbusch and R.D. Larrabee gave helpful comments on an earlier version of this report.

REFERENCES

Bosma, J. and Vugts, J. H. (1981), Wave Kinematics and Fluid Loading in Irregular Waves, *Intern. Symposium on Hydrodynamics in Ocean Eng.*, Trondheim.

Chappelear, J. E. (1961), The Direct Numerical Calculation of Wave Properties, *J. Geophys. Res.*, **66**, 501.

Daemrich, K. F., Eggert, W. D., and Kohlhase, S. (1980), Investigations on Irregular Waves in Hydraulic Models, *Proc. 17th Coastal Eng. Conf.*, Sydney.

Forristall, G.Z. (1981), Kinematics of Directionally Spread Waves, *Proc. Directional Wave Spectra Applications*, Am. Soc. Civil Engr., Berkeley.

Forristall, G.Z. (1985), Irregular Wave Kinematics From a Kinematic Boundary Condition Fit (KBCF), *Applied Ocean Res.*, **7**, 202–212.

Forristall, G.Z. and Hamilton, R. C (1978), Current Measurements in Support of Fixed Platform Design and Construction, *Proc. of a Working Conference on Current Measurement*, Univ. Deleware, Newark.

Forristall, G. Z., Ward, E. G, Cardone, V.J., and Borgman, L.E. (1978), The Directional Spectra and Kinematics of Surface Gravity Waves in Tropical Storm Delia, *J. Phys. Oceanogr.*, **8**, 888–909.

Longuet-Higgins, M. S. (1963), The Effect of Non-Linearities on Statistical Distributions in the Theory of Sea Waves, *J. Fluid Mech.*, **17**, 459-480.

Mariners Weather Log (1982), North Atlantic Weather Log, **26**, 81.

Rodenbusch, G. and Forristall, G.Z. (1986), An Empirical Model for Random Directional Wave Kinematics Near the Free Surface, *Proc. 18th Annual Offshore Tech. Conf.*, OTC Paper 5097, Houston.

Sharma, J. N. and Dean, R. G. (1979), Development and Evaluation of a Procedure for Simulating a Random Directional Second Order Sea Surface and Associated Wave Forces, *Ocean Eng. Report 20*, Univ. Deleware, Newark.